Carbohydrate Polymers 121 (2015) 302–308

Contents lists available at ScienceDirect

Carbohydrate Polymers

journal homepage: www.elsevier.com/locate/carbpol

Chitosan conjugation: A facile approach to enhance the cell viability of LaF_3:Yb,Er upconverting nanotransducers in human breast cancer cells

Sethuraman Gayathri [a], Oriparambil Sivaraman Nirmal Ghosh [a], P. Sudhakara [b], Annamraju Kasi Viswanath [a,*]

[a] Nanophotonics and Nanoelectronics Research Laboratory, Centre for Nanoscience and Technology, Madanjeet School of Green Energy Technologies, Pondicherry University, Kalapet, Puducherry 605014, India
[b] CSIR—Central Leather Research Institute, Regional Centre for Extension and Development, Leather Complex, Jalandhar 144021, Punjab, India

ARTICLE INFO

Article history:
Received 26 August 2014
Received in revised form
29 November 2014
Accepted 2 December 2014
Available online 31 December 2014

Keywords:
Chitosan
Surface functionalization
Natural biopolymer
Enhanced cell viability
Upconverting nanotransducers
Cancer therapy

ABSTRACT

In this study, chitosan functionalized LaF_3:Yb,Er upconverting nanotransducers (UCNTs) with controlled size and shape have been successfully synthesized by a facile one pot precipitation method. The chitosan encapsulated UCNTs show bright upconversion fluorescence upon excitation with 974 nm NIR region. The average crystallite size of UCNTs about 7.6 nm was achieved using chitosan mediated synthesis. The FTIR result confirms the chitosan coating over the LaF_3:Yb,Er nanoparticles. Due to the surface modification using natural biopolymer chitosan, the as-prepared nanocrystals show excellent biocompatibility even at high dose at 200 μg/ml. To the best of our knowledge the presented work is the first report on in vitro analysis of chitosan conjugated LaF_3:Yb,Er upconverting nanocrystals in human breast (MCF-7) cancer cells. These nanotransducers can be used as luminescent probes for bioimaging and deep tissue cancer therapeutic applications.

1. Introduction

Polymer functionalized nanoparticles are having tremendous potential in bioimaging, in vivo drug delivery and various biomedical applications. Synthetic and biodegradable polymers are widely used as nanovehicles for controlled delivery of drugs and functional biological macromolecules (Janeesh, Sami, Dhanya, Sivakumar, & Abraham, 2014). The research on the toxicity of the polymer nanoparticles play a key role in biomedical applications. Chitosan is one of the most widely used natural polymers in nanotechnology for the surface modification of nanomaterials. The chitosan encapsulation of nanomaterials provides various advantages including water solubility, biocompatibility, biodegradability (Muzzarelli, 1988; Jayakumar, Menon, Manzoor, Nair, &Tamura, 2010), antibacterial activity (Foudaa, El-Aassarc, & Al-Deyaba, 2013), low toxicity and wound healing (Ueno et al., 1999) properties. Chitins and chitosan derivatives have unique characteristics which facilitates the regeneration of animal and human tissues (Muzzarelli, 2009). The chemical and pharmaceutical perspectives of chitosan and its derivatives were already reported (Kumar, Muzzarelli, Muzzarelli, Sashiwa, & Domb, 2004). Chitosan functionalized rare earth nanoparticles are emerging materials for targeted drug delivery and imaging of cancer cells (Mathew et al., 2010). Chitosan modified nanoparticles are also used for advanced magnetic resonance imaging of sub cellular biocomponents (Darras, Nelea, Winnik, & Buschmann, 2010). Recently lot of efforts have been made by international scientists community to develop chitosan and other polymer conjugated fluorescent nanomarkers and multifunctional nanohybrids for bio-labeling (Yan et al., 2011; Saeed et al., 2014), photodynamic therapy (Li et al., 2011), targeted drug delivery (Chen et al., 2013; Anitha et al., 2011), cancer imaging, therapy (Jayasree, Sasidharan, Koyakutty, Nair, & Menon, 2011) and biomedical applications (Nidhin et al., 2014; Reddy & Gomes, 2014).

Lanthanum fluoride based upconverting nanoparticles are identified as one of the most efficient host matrices for upconversion fluorescent systems due to their low phonon vibration energy about 350 cm^{-1} (Stouwdam, Hebbink, Huskens, & Veggel, 2003). Therefore, LaF_3 is extensively used as a host matrix to dope rare earth ions for developing upconverting nanotransducers (UCNTs). UCNTs exhibit unique spectral property to transform the

* Corresponding author. Tel.: +91 8098058957.
E-mail addresses: v_kasi@hotmail.com, nnrlcnstpu@gmail.com (A.K. Viswanath).

http://dx.doi.org/10.1016/j.carbpol.2014.12.022
0144-8617/

infra-red (IR) light into visible and stable fluorescence. Generally, all the biomolecules absorb minimally in the NIR window, UCNTs can be excited using low energy IR signals which are transparent for biomolecules. In this regard, rare earth doped upconversion nanocrystals are of particular interest to be used in detection of low abundant sub cellular components, photocontrollable gene expressions, gene delivery and tracking, deep tissue imaging and targeted photodynamic therapy against cancer (Yang, 2014; Gayathri et al., 2015). Due to the +3 valency and similar ionic radii, rare earth ion doping (RE: Eu^{3+}, Tb^{3+}, Yb^{3+}, Er^{3+}, Tm^{3+}, Ho^{3+}, Gd^{3+} and Sc^{3+}) in LaF_3 matrix would not suffer from any thermodynamic and kinetic hindrance, which induce the distortion in either crystal lattice or in the stoichiometry (Chao, Lingdong, Yawen and Chunhua, 2010). Lanthanide nanoparticles like LaF_3: Yb,Er were having the potential advantages of narrow emission peak, large stokes shifts, long life times, superior photostability and high quantum yields. This is obtained due to the 4f or 5f electronic structure of rare earth dopant ions (Wright, 1976; Heer, Kompe, Gudel, & Haase, 2004; Vetrone, Boyer, Capobianco, Speghini, & Bettinelli, 2003). In the field of luminescent biolabeling, UCNFs are considered due to their attractive optical and chemical features such as large effective stokes shifts as well as high resistance to photobleaching, blinking and photochemical degradation (Niggli & Egger, 2004). However the water solubility and cytotoxicity of the LaF_3:Yb,Er UCNTs are the major issues to be rectified to utilize the full potential of these novel materials for cancer therapy of deeply seated cancers. Synthesis of water soluble poly amino acid functionalized LaF_3:Yb,Er nanocrystals using octadecylene as a medium and oleic acid as surfactant has been recently reported (Chang & Maoguo, 2014). While synthesizing rare earth doped lanthanide UCNTs, organic surfactants are often used as ligands to control the particles growth and to stabilize the particles against aggregation, hence the nanocrystals are not soluble in water. Also the bioconjugation of UCNTs require further surface functionalization, hence their biological applications has been limited (Chen, Herricks, & Xia, 2005; Qin et al., 2008; Li & Zhang, 2008; Wang, Abbineni, Clevenger, Mao, & Xu, 2011).

In this present study we report a facile one pot synthesize of chitosan capped hydrophilic LaF_3:Yb,Er UCNTs with high biocompatibility by precipitation method. The natural biopolymer, chitosan was used as a capping agent which eliminates further surface functionalization on the nanoparticles to enhance the conjugation functionalities with biomolecules for applications in advanced cancer therapy. The natural biopolymer chitosan controls the particles growth and stabilizes the nanoparticles against aggregation in solutions. Cell viability assessment has been done in MCF-7 cells to investigate the toxicity of the developed UCNTs. It is found that even at high administrated dosage of 200 μg/ml, the UCNTs show excellent cell viability, which is much higher than the standard concentration of biomarkers used for cell labeling at present (Ruichan et al., 2014). To the best of our knowledge, this is the first report on the cytotoxicity assessment of chitosan functionalized LaF_3:Yb,Er UCNTs in human breast cancer cells.

2. Experimental

2.1. Materials

Lanthanum chloride hydrate ($LaCl_3{\cdot}7H_2O$, 99.9%), ammonium fluoride (NH_4F, 98+%), ytterbium oxide (Yb_2O_3, 99.9%) and erbium oxide (Er_2O_3, 99.9%), were purchased from Sigma-Aldrich. Chitosan (degree of deacetylation (DDA) 95%) was purchased from Fluka. All of the reagents were used as received, without further purification. 0.2 M of lanthanide precursor stock solution was prepared by dissolving $LaCl_3{\cdot}7H_2O$ in deionized water. 0.2 M of $YbCl_3$, $ErCl_3$ precursors were prepared by dissolving the corresponding oxides into HCl solution. The chitosan stock solution of 1 wt% was prepared in 0.05 M HCl solution.

2.2. One pot synthesis of chitosan functionalized LaF_3:Yb^{3+}, Er^{3+}

The chitosan encapsulated LaF_3:Yb,Er nanocrystals were synthesized through a simple precipitation method. In a typical procedure, 8 ml of $LaCl_3$, 1.8 ml of $YbCl_3$ and 0.2 ml of $ErCl_3$ solutions were added into the round bottom flask and stirred for 1 h. 25 ml of chitosan solution was added to the former solution and stirred for 15 min until the homogenous solution appeared. After stirring, required amount of NH_4F is injected into the solution. The mixture was consequently heated to 70 °C for 2 h under stirring. The nanocrystals were collected by centrifugation and washed with ethanol and deionized water. Finally, the obtained nanocrystals were kept at 110 °C for 12 h in hot air oven to remove the impurities left in the final product.

2.3. In vitro viability of chitosan functionalized LaF_3:Yb,Er UCNTs

The human breast cancer cell line (MCF-7) was obtained from National Centre for Cell Science (NCCS), Pune and grown in Eagles Minimum Essential Medium containing 10% fetal bovine serum (FBS). The cells were maintained at 37 °C, 5% CO_2, 95% air and 100% relative humidity. Maintenance cultures were passaged weekly, and the culture medium was changed twice a week. The monolayer cells were detached with trypsin–ethylene-diamine tetra-acetic acid (EDTA) to make single cell suspensions and viable cells were counted using a hemocytometer and diluted with medium containing 5% FBS to give final density of 1×10^5 cells/ml. One hundred microliters per well of cell suspension were seeded into 96-well plates at plating density of 10,000 cells/well and incubated to allow for cell attachment at 37 °C, 5% CO_2, 95% air and 100% relative humidity. After 24 h the cells were treated with serial concentrations of the test samples. They were initially dissolved in phosphate buffered saline (PBS) and an aliquot of the sample solution was diluted to twice the desired final maximum test concentration with serum free medium. Four Additional two fold serial dilutions were made to provide a total of five sample concentrations. Aliquots of 100 μl of these different sample dilutions were added to the appropriate wells already containing 100 μl of medium, so as to obtain the required final sample concentrations. Following sample addition, the plates were incubated for an additional 48 h at 37 °C, 5% CO_2, 95% air and 100% relative humidity. The medium without samples were served as control and triplicate was maintained for all concentrations.

After 48 h of incubation, 15 μl of 3-[4,5-dimethylthiazol-2-yl]2,5-diphenyltetrazolium bromide (MTT-5 mg/ml) in phosphate buffered saline (PBS) was added to each well and was incubated at 37 °C for 4 h. The medium with MTT was then flicked off and the resultant formazan crystals were dissolved in 100 μl of DMSO and the subsequent absorbance value was measured using (570 nm) micro plate reader. The percentage cell viability was then calculated with respect to control as

$$\%\,\text{cell viability} = \frac{[A]\text{test}}{[A]\text{control}} \times 100$$

2.4. Characterization

Powder X-ray diffraction (XRD) was carried out on a Rigaku Ultima IV diffractometer equipped with Cu_α (1.5406 Å) X-ray source. The surface morphology, chemical composition and elemental profile of the prepared samples were taken by using scanning electron microscope (SEM) (Model-Hitachi S3400N) with energy dispersive X-ray (EDAX) (Make-Thermo scientific)

attachment. High-resolution field emission transmission electron microscopy (FETEM) and selected area electron diffraction (SAED) were performed on a JEOL JEM-2100F TEM operating at 200 kV. The nanocrystals for analysis were prepared by dispersing the nanocrystals in ethanol and dripped over a copper specimen grid coated with a permeable carbon film and allowed to dry. Surface texture and 3D profile of the samples were reconstructed from the scanning electron micrographs using analytical software 'Mountains Map®SEM'. Fourier transform infrared (FTIR) spectra were recorded by using (Model Thermo Nicolet-6700) FTIR spectrometer. Photoluminescence (PL) measurements of the samples at room temperature were recorded with a Horiba-Fluoromax IV fluorescence spectrometer.

3. Results and discussion

3.1. Structure, morphology and elemental analysis of the UCNTs

The formation of crystalline phase in the prepared sample was confirmed by powder XRD measurements.

Fig. 1 shows X-ray diffractogram of the powder LaF_3: Yb^{3+}, Er^{3+} nanocrystals. The diffraction patterns agree well with the standard JCPDS file (32-0483), which confirmed the formation of hexagonal phase. Broadened peaks in the LaF_3:Yb^{3+}, Er^{3+} XRD pattern imply small crystallite size. The average crystalline size of the powders was calculated to be about 7.6 nm according to the Debye–Scherrer equation $D = 0.89\lambda/\beta\cos\theta_B$, where D represents the crystallite size (nm), λ is the wavelength of the target used, θ_B is half the diffraction angle and β is full-width at half maximum for this angle. This result shows that the powder product formed during the typical process yielded distinct LaF_3 XRD peaks without the requirement of any further heat treatment.

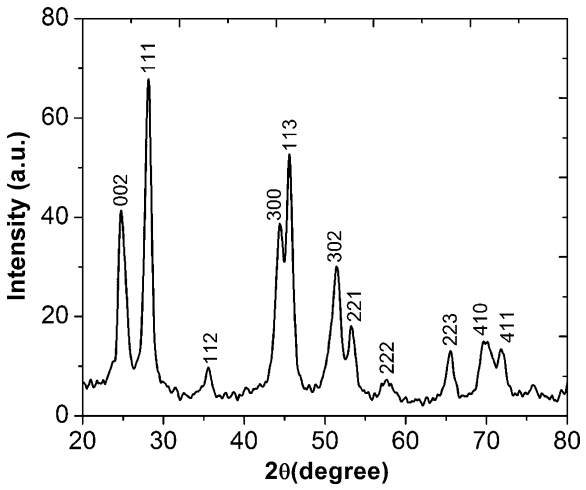

Fig. 1. X-ray powder diffraction pattern of chitosan capped LaF_3:Yb,Er nanocrystals.

Scanning electron microscopy analysis was carried out to investigate the surface morphology of synthesized UCNTs.

Fig. 2(a, c and d) shows the SEM images of the LaF_3:Yb,Er capped with natural polymer chitosan. The low magnification scanning electron micrograph shows the spherical surface of the agglomerated UCNTs. Fig. 2(b) shows the homogeneous surface texture

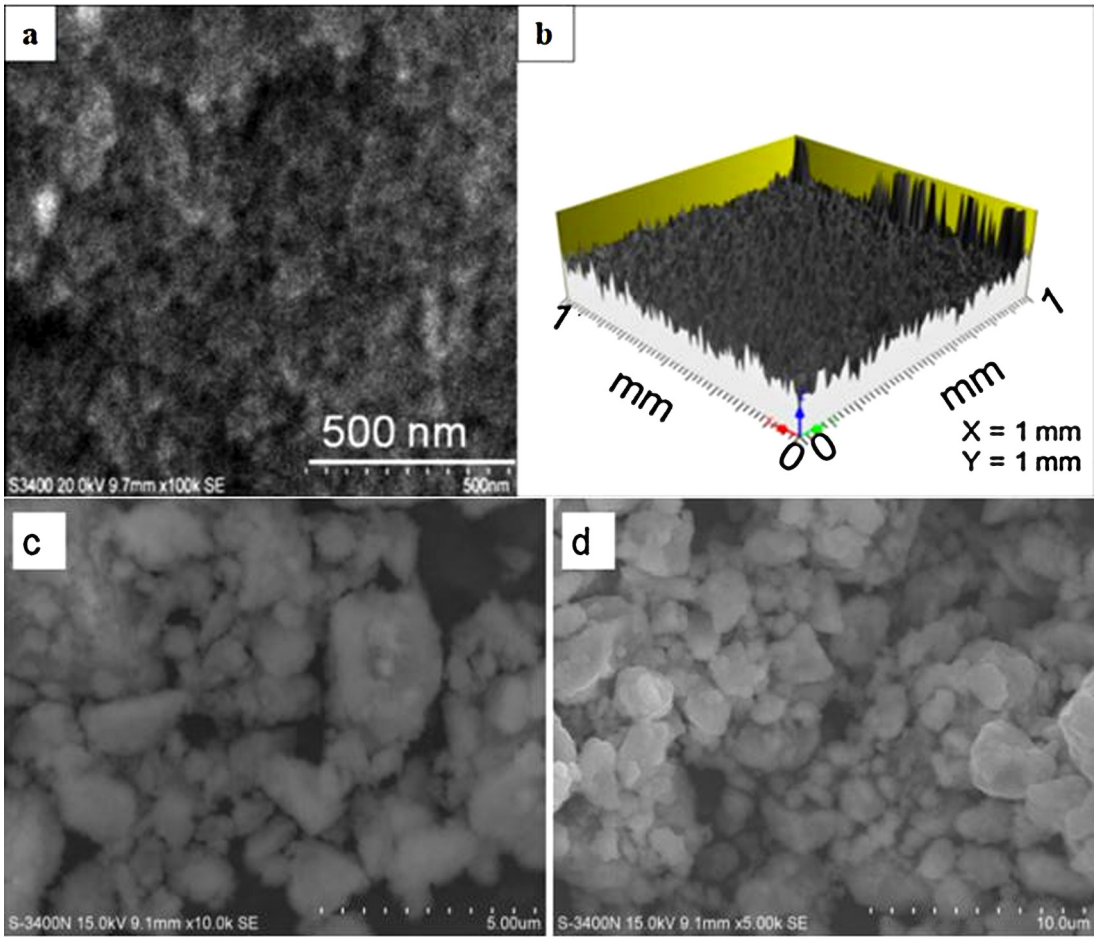

Fig. 2. (a, c and d) SEM images of LaF_3:Yb,Er capped with chitosan. (b) The surface texture of LaF_3:Yb,Er capped with chitosan constructed using Mountains Map®SEM.

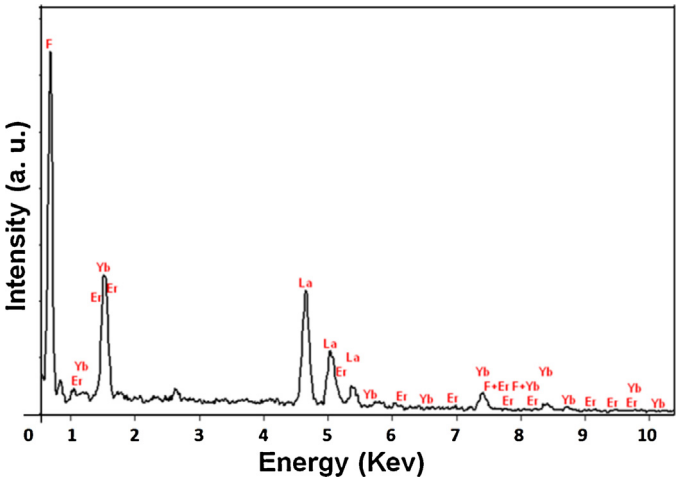

Fig. 3. EDX spectrum of chitosan capped LaF_3:Yb,Er nanocrystals.

of the UCNTs constructed by the extracted data points from SEM image using Mountains Map®SEM analysis software.

Energy dispersive X-ray spectroscopy (EDX) reveals the presence of La, F, Yb and Er elements in the prepared nanocrystals. Fig. 3 shows the EDX spectra and it was confirmed that the Yb and Er ions were existing in the prepared sample. For LaF_3:18%Yb2%Er nanocomposite, the elemental composition of the particles were found to be $La_{0.77}Yb_{0.20}Er_{0.02}F_3$ from the EDX analysis result.

Transmission electron microscopy was carried out for the in-depth understanding about the structure of single LaF_3:Yb,Er nanoparticle. High magnification TEM images shown in Fig. 4(a–c) divulges the uniform size of nanocrystals randomly arranged to form pure LaF_3 nanoparticles. The adjacent nanocrystals are joined together to form LaF_3:Yb,Er nanoparticles with size distribution less than 10 nm and which is in agreement with the average crystallite size obtained from X-ray diffractogram. Fig. 4(d) shows the SAED pattern of LaF_3 nanocrystals. The obtained diffraction rings can be indexed to the (0 0 2), (1 1 1), (3 0 0) and (1 1 3) planes of LaF_3 nanocrystals and it suggest that the constituent nanocrystals are randomly aligned to form LaF_3 nanoparticle. Fig. 4(f) shows the HRTEM image of LaF_3 nanoparticles. The distance of adjacent lattice fringes of LaF_3 nanocrystals is determined to be about 0.31 nm, which well matches with the $d_{1\,1\,1}$ spacing of hexagonal phase LaF_3 host. Fig. 4(e) shows that the nanocrystals are aggregated due to the capping effect of chitosan to form LaF_3:Yb,Er nanoparticles with size distribution less than 50 nm. From Fig. 4(e) the average thickness of the chitosan coating was determined as 6 nm.

3.2. Upconversion luminescence

Fig. 5 shows the upconversion emission spectrum of pure LaF_3:Yb,Er nanoparticles upon excitation at 974 nm. Firstly the electrons in the ground state were excited to the intermediate state $^4I_{11/2}$ of Er^{3+} and then to the $_4F^{7/2}$ state through a consecutive energy transfer from $_2F^{5/2}$ state (excited energy level) of Yb^{3+}. Successively, those electrons undergo a non-radiative decay to the respective lower excited state energy levels $_4H^{11/2}$ and $_4S^{3/2}$. From these energy levels the electrons return to the ground state by releasing energy in the form of green light due to the upconversion energy transfer process. The observed emission peaks centered at 532 nm, 545 nm and 660 nm are assigned to the transitions of $^2H_{11/2}$ to $^4I_{15/2}$, $^4S_{3/2}$ to $^4I_{15/2}$ and $^4F_{9/2}$ to $^4I_{15/2}$, respectively.

Fig. 6 illustrates the upconversion emission spectrum of chitosan capped LaF_3:Yb,Er nanoparticles upon excitation at 974 nm. The photoluminescence spectrum of chitosan capped UCNTs shows similar emission peaks obtained for pure LaF_3:Yb,Er as depicted in Fig. 5. The photoluminescence spectra presented in Figs. 5 and 6 clearly show that there is a quenching in intensity of the emission spectrum of chitosan capped LaF_3:Yb,Er UCNTs in comparison with that of pure LaF_3:Yb,Er UCNTs. This luminescence quenching is observed due to the reduction in radiative recombination process during the upconversion energy transfer process caused by the surface passivation effect of chitosan polymer. The effect of chitosan capping leads to the formation of agglomerated LaF_3:Yb,Er UCNTs which result in the quenching of photoluminescence intensity. Moreover, the size of the nanoclusters were found to be increased due to the agglomeration of the nanoparticles which is in good agreement with the TEM measurement.

3.3. FTIR analysis

Fourier transform infrared (FT-IR) measurements were carried out to identify the functional groups existing on the surface of the nanocrystals. Fig. 7(a–c) shows the FT-IR spectra of the as prepared LaF_3:Yb,Er nanocrystals, pure chitosan and chitosan capped LaF_3:Yb,Er nanocrystals, respectively. The absorption bands in the regions of 700–1000 cm^{-1} and 1580–1650 cm^{-1} are due to the corresponding C—H bending vibrations and amide bonds present in the capping agent chitosan. The unique peak in Fig. 7(c) around 1636 cm^{-1} should be attributed to the N—H bending vibration. This reveals the presence of amine functional group on the chitosan encapsulated nanoparticles which further confirm the effective capping of chitosan polymer over the surface of the nanoparticles.

The absorption band in the region above 3000 cm^{-1} is due to the water content because of isolated O—H group, which indicates that water solubility of the LaF_3:Yb,Er UCNTs increases due to the chitosan capping. The natural biopolymer chitosan provides the anchoring points for transition metal ions to form a complex with amino groups. These amino group complexes having unoccupied coordination points which can be further conjugated with biomolecules. In this regard the chitosan capped LaF_3:Yb,Er UNCTs possess great ability to link with biomolecules which enhances the cell viability.

3.4. Cell viability and toxicity studies in MCF-7 cells

LaF_3 nanoparticles coated with chitosan were incubated in physiological conditions (at 37 °C, 5% CO_2 and 100% relative humidity) of MCF-7 cell monolayer for 24 h. Different concentrations of nanoparticles have been chosen: 12.5, 25, 50, 100 and 200 μg/ml. After incubation, the samples were washed three times with IXPBS to remove unbound particles. MCF-7 cell monolayer culture without addition of nanoparticles was used as a control. Remaining cells were counted after incubation using a hemocytometer. The obtained results show that the respective cell viabilities (99.81, 99.06, 98.69 and 95.22%) were achieved for corresponding concentrations (12.5, 25, 50 and 100 μg/ml) upon incubating the cells with chitosan capped UCNTs. When the concentration of the chitosan/UCNTs was increased to 200 μg/ml, the cell viability reduces up to 79.60%. The bare LaF_3:Yb,Er nanoparticles up to the concentration of 60 μg/ml did not show any toxic behavior. When concentration of the nanoparticles exceed, it shows remarkable toxicity which in turn reduces the cell viability. In case of chitosan coated nanoparticles there is no significant toxicity up to the dose rate of 100 μg/ml. These data confirms that there is no significant cytotoxicity for chitosan coated nanoparticles under the high drug dosage up to 200 μg/ml in human breast cancer cells even after 48 h of incubation.

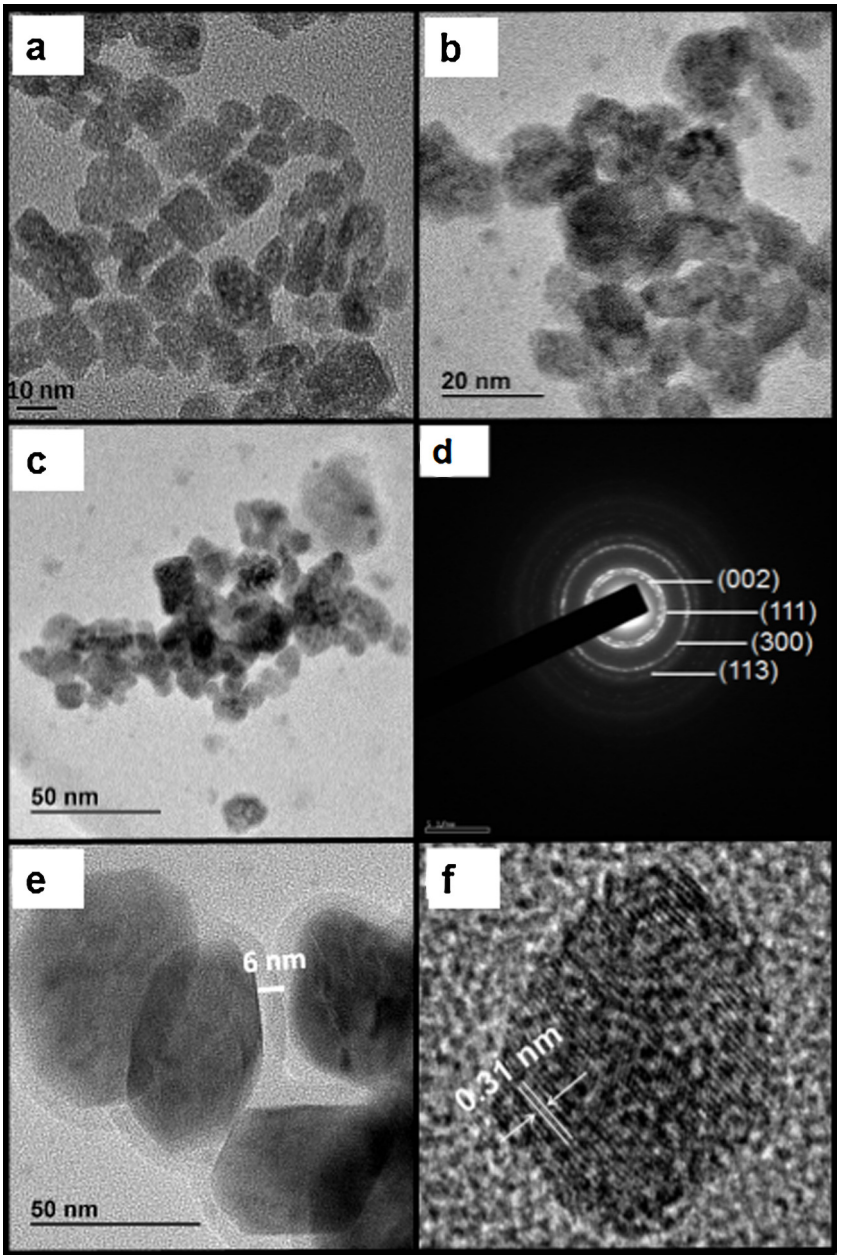

Fig. 4. (a, b and c) Are respective TEM images of LaF_3:Yb,Er nanoparticles. (e) Is the TEM image of chitosan capped LaF_3:Yb,Er nanoparticles. (f and d) Are the high resolution TEM image and *in situ* SAED pattern of selective nanocrystals, respectively.

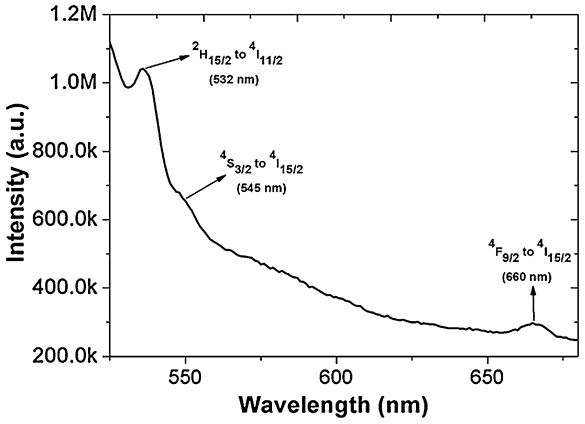

Fig. 5. Photoluminescence spectrum of pure LaF_3:Yb,Er UCNTs.

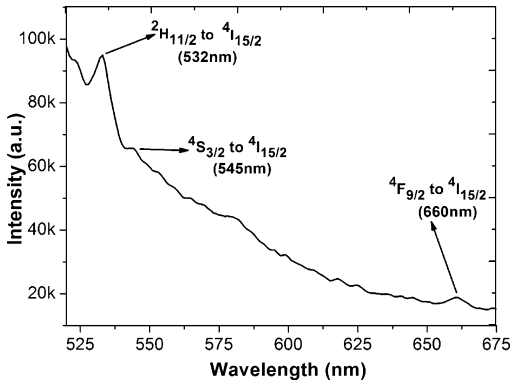

Fig. 6. Photoluminescence spectrum of chitosan functionalized LaF_3:Yb,Er UCNTs.

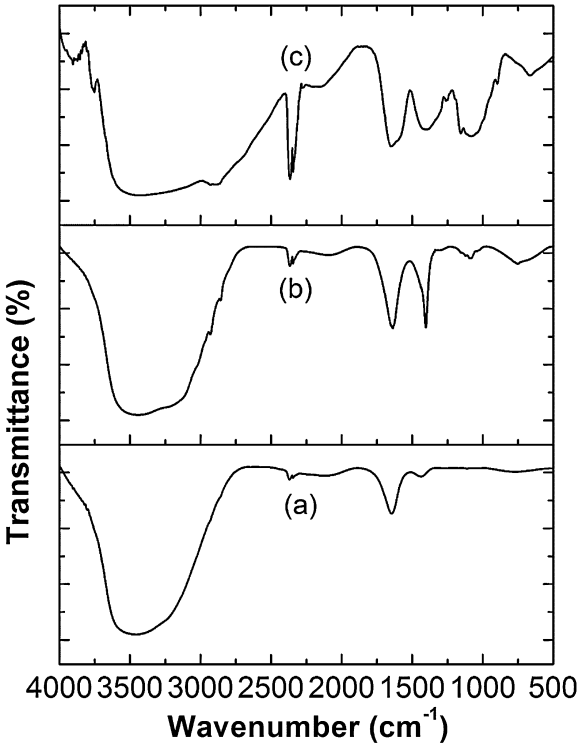

Fig. 7. FT-IR spectra of (a) pure nanoparticles, (b) chitosan capped LaF_3:Yb,Er nanocrystals and (c) pure chitosan.

Currently chemotherapy and conventional therapeutic techniques are used for the breast cancer treatment. Upconversion transducers mediated photodynamic therapy (PDT) can be a novel alternative to these conventional techniques. PDT was usually administrated by using deep penetrating bio-transparent NIR signal to trigger the upconverting transducer to activate the cancer drugs. So far very limited information are available on in vitro cytotoxicity investigations of surface modified UCNTs. To the best of our knowledge the cell viability of chitosan coated LaF_3:Yb,Er upconversion nanotransducers on MCF-7 cells nowhere else reported. The cytotoxicity studies on MCF-7 cells were confirmed that the developed upconversion nanoparticles are suitable for theranostic applications.

4. Conclusion

In conclusion, chitosan capped LaF_3:Yb,Er UCNTs were synthesized using a facile one pot precipitation method. The XRD analysis confirmed the formation of LaF_3 hexagonal phase crystal structure with an average crystalline size of 7.6 nm. The nanocrystals were water soluble and highly biocompatible due to the surface functionalization using biopolymer chitosan. Under 974 nm NIR excitation, the synthesized UCNTs yielded a strong green fluorescent upconversion emission. The authors believe that the presented investigations on cytotoxicity of LaF_3:Yb,Er in MCF-7 cells a substantial step towards the clinical application of upconverting transducers in breast cancer therapeutics.

Acknowledgements

S. Gayathri and O. S. N. Ghosh would like to thank Dr. S. Kannan for XRD analysis. The authors thankfully acknowledge the advanced material characterization facility provided by Centre for Nanoscience and Technology and Central Instrumentation Facility, Pondicherry University, India.

References

Anitha, A., Deepa, N., Chennazhi, K. P., Nair, S. V., Tamura, H., & Jayakumar, R. (2011). Development of mucoadhesive thiolated chitosan nanoparticles for biomedical applications. *Carbohydrate Polymers*, *83*, 66–73.

Chang, G., & Maoguo, L. (2014). Synthesis and cell imaging of LaF_3 nanocrystals with small particle size and novel upconversion luminescence. *Acta Chimica Sinica*, *72*, 215–219.

Chao, Z., Lingdong, S., Yawen, Z., & Chunhua, Y. (2010). Rare earth upconversion nanophosphors: Synthesis, functionalization and application as biolabels and energy transfer donors. *Journal of Rare Earths*, *28*, 807–819.

Chen, J., Herricks, T., & Xia, Y. (2005). Polyol synthesis of platinum nanostructures: Control of morphology through the manipulation of reduction kinetics. *Angewandte Chemie International Edition*, *44*, 2589–2592.

Chen, T., Zhao, T., Wei, D., Wei, Y., Li, Y., & Zhang, H. (2013). Core–shell nanocarriers with ZnO quantum dots-conjugated Au nanoparticle for tumor-targeted drug delivery. *Carbohydrate Polymers*, *92*, 1124–1132.

Darras, V., Nelea, M., Winnik, F. M., & Buschmann, M. D. (2010). Chitosan modified with gadolinium diethylenetriaminepentaacetic acid for magnetic resonance imaging of DNA/chitosan nanoparticles. *Carbohydrate Polymers*, *80*, 1137–1146.

Foudaa, M. M. G., El-Aassarc, M. R., & Al-Deyaba, S. S. (2013). Antimicrobial activity of carboxymethyl chitosan/polyethylene oxide nanofibers embedded silver nanoparticles. *Carbohydrate Polymers*, *92*, 1012–1017.

Gayathri, S., Ghosh, O. S. N., Viswanath, A. K., Sudhakara, P., Reddy, M. J. K., & Shanmugharaj, A. M. (2015). Synthesis of YF_3: Yb,Er upconverting nanofluorophores using chitosan and their cytotoxicity in MCF-7 cells. *International Journal of Biological Macromolecules*, *72*, 1308–1312.

Heer, S., Kompe, K., Gudel, H. U., & Haase, M. (2004). Highly efficient multicolour upconversion emission in transparent colloids of lanthanide doped $NaYF_4$ nanocrystals. *Advanced Materials*, *16*, 2102–2105.

Janeesh, P. A., Sami, H., Dhanya, C. R., Sivakumar, S., & Abraham, A. (2014). Biocompatibility and genotoxicity studies of polyallylamine hydrochloride nanocapsules in rats. *RSC Advanced*, *4*, 24484–24497.

Jayakumar, R., Menon, D., Manzoor, K., Nair, S. V., & Tamura, H. (2010). Biomedical applications of chitin and chitosan based nanomaterials—A short review. *Carbohydrate Polymers*, *82*, 227–232.

Jayasree, A., Sasidharan, S., Koyakutty, M., Nair, S., & Menon, D. (2011). Mannosylated chitosan–zinc sulphide nanocrystals as fluorescent bioprobes for targeted cancer imaging. *Carbohydrate Polymers*, *85*, 37–43.

Kumar, M. N. V. R., Muzzarelli, R. A. A., Muzzarelli, C., Sashiwa, H., & Domb, A. J. (2004). Chitosan chemistry and pharmaceutical perspectives. *Chemical Reviews*, *104*, 6017–6084.

Li, L., Bae, B. C., Tran, T. H., Yoon, K. H., Na, K., & Huh, K. M. (2011). Self-quenchable biofunctional nanoparticles of heparin–folate-photosensitizer conjugates for photodynamic therapy. *Carbohydrate Polymers*, *86*, 708–715.

Li, Z. Q., & Zhang, Y. (2008). An efficient and user friendly method for the synthesis of hexagonal phase $NaYF_4$:Yb, Er/Tm nanocrystals with controllable shape and upconversion fluorescence. *Nanotechnology*, *19*, 345606–345610.

Mathew, M. E., Mohan, J. C., Manzoor, K., Nair, S. V., Tamura, H., & Jayakumar, R. (2010). Folate conjugated carboxymethyl chitosan–manganese doped zinc sulphide nanoparticles for targeted drug delivery and imaging of cancer cells. *Carbohydrate Polymers*, *80*, 442–448.

Muzzarelli, R. A. A. (1988). Carboxymethyl chitins and chitosans. *Carbohydrate Polymers*, *8*, 1–21.

Muzzarelli, R. A. A. (2009). Chitins and chitosans for the repair of wound, skin, nerve, cartilage and bone. *Carbohydrate Polymers*, *76*, 167–182.

Nidhin, M., Vedhanayagam, M., Sangeetha, S., Kiran, M. S., Nazeer, S. S., Jayasree, R. S., et al. (2014). Fluorescent nano networks: A novel bioalley for collagen scaffolds and Tissue Engineering. *Scientific Reports*, *4*, 1–10.

Niggli, E., & Egger, M. (2004). Applications of multi-photon microscopy in cell physiology. *Frontiers in Bioscience*, *9*, 1598–1610.

Qin, R., Song, H., Pan, G., Hu, L., Yu, H., Li, S., et al. (2008). Polyol-mediated syntheses and characterization of $NaYF_4$, $NH_4Y_3F_{10}$ and YF_3 nanocrystals/submicrocrystals. *Materials Research Bulletin*, *43*, 2130.

Reddy, K. R., & Gomes, V. G. (2014). Nanoparticles for clinical applications. In R. S. Chaughule, & A. R. Kapdi (Eds.), *Nanoparticles for catalysis, energy and drug delivery*. Los Angeles, CA: American Scientific Publishers (Chapter 11).

Ruichan, L., Gai, S., Dai, Y., He, F., Niu, N., & Yang, P. (2014). Surfactant-free synthesis, luminescent properties, and drug-release properties of LaF_3 & $LaCO_3F$ hollow microspheres. *Inorganic Chemistry*, *53*, 998–1008.

Saeed, S. E., El-Molla, M. M., Hassan, M. L., Bakir, E., Abdel-Mottaleb, M. M. S., & Abdel-Mottaleb, M. S. A. (2014). Novel chitosan–ZnO based nanocomposites as luminescent tags for cellulostic materials. *Carbohydrate Polymers*, *99*, 817–824.

Stouwdam, J. W., Hebbink, G. A., Huskens, J., & van Veggel, F. C. J. M. (2003). Lanthanide-doped nanoparticles with excellent luminescent properties in organic media. *Chemistry of Materials*, *15*, 4604–4616.

Ueno, H., Yamada, H., Tanaka, I., Kaba, N., Matsuura, M., Okumura, M., et al. (1999). Accelerating effects of chitosan for healing at early phase of experimental open wound in dogs. *Biomaterials*, *20*, 1407–1414.

Vetrone, F., Boyer, J. C., Capobianco, J. A., Speghini, A., & Bettinelli, A. M. (2003). Effect of Yb^{3+} co-doping on the upconversion emission in nanocrystalline Y_2O_3:Er^{3+}. *The Journal of Physical Chemistry B*, *107*, 1107–1112.

Wang, M., Abbineni, G., Clevenger, A., Mao, C., & Xu, S. (2011). Upconversion nanoparticles: Synthesis, surface modification and biological applications. *Nanomedicine: Nanotechnology, Biology and Medicine*, *7*, 710–729.

Wright, J. C. (1976). Upconversion and excited state energy transfer in rare earth doped materials. In F. K. Fong (Ed.), *Radiationless processes in molecules and crystals* (pp. 239–292). Berlin, Heidelberg, New York: Springer-Verlag.

Yan, E., Wang, C., Wang, S., Sun, L., Wang, Y., Fan, L., et al. (2011). Synthesis and characterization of fluorescent chitosan–ZnO hybrid nanospheres. *Materials Science and Engineering B*, *176*, 458–461.

Yang, Y. (2014). Upconversion phosphores for use in bioimaging, therapy, drug delivery and bioassays. *Microchimica Acta*, *181*, 263–294.